

## Article

# Fabrication of Ternary MoS<sub>2</sub>/CdS/Bi<sub>2</sub>S<sub>3</sub>-Based Nano Composites for Photocatalytic Dye Degradation

Asif Nazir <sup>1,\*</sup>, Muhammad Suleman Tahir <sup>2,3</sup>, Ghulam Mustafa Kamal <sup>1</sup>, Xu Zhang <sup>4,5,6,\*</sup>,  
Muhammad Bilal Tahir <sup>7</sup>, Bin Jiang <sup>4,5,6</sup> and Muhammad Safdar <sup>1</sup>

<sup>1</sup> Institute of Chemistry, Faculty of Natural and Applied Sciences, Khwaja Fareed University of Engineering and Information Technology, Rahim Yar Khan 64200, Pakistan

<sup>2</sup> Institute of Chemical and Environmental Engineering, Khwaja Fareed University of Engineering and Information Technology, Rahim Yar Khan 64200, Pakistan

<sup>3</sup> Department of Chemical Engineering, University of Gujrat, Gujrat 50700, Pakistan

<sup>4</sup> Optics Valley Laboratory, Wuhan 430074, China

<sup>5</sup> State Key Laboratory of Magnetic Resonance and Atomic Molecular Physics, Key Laboratory of Magnetic Resonance in Biological Systems, National Center for Magnetic Resonance in Wuhan, Wuhan Institute of Physics and Mathematics, Innovation Academy for Precision Measurement Science and Technology, Chinese Academy of Sciences, Wuhan 430071, China

<sup>6</sup> Wuhan National Laboratory for Optoelectronics, Huazhong University of Science and Technology, Wuhan 430071, China

<sup>7</sup> Institute of Physics, Khwaja Fareed University of Engineering and Information Technology, Rahim Yar Khan 64200, Pakistan

\* Correspondence: asifnazir723@gmail.com (A.N.); zhangxu@wipm.ac.cn (X.Z.); Tel.: +92-333-5792575 (A.N.)

**Abstract:** The synthesis and design of low-cost visible-light-active catalysts for the photodegradation of organic dyes have been regarded as an efficient way to use solar energy in addressing environmental issues. We report the fabrication of MoS<sub>2</sub>/CdS nanoparticles functionalized with Bi<sub>2</sub>S<sub>3</sub> nanoflakes. The ternary composites of “MoS<sub>2</sub>/CdS/Bi<sub>2</sub>S<sub>3</sub>” were synthesized in situ by a hydrothermal method at different temperatures. The changes in structural, optical, and morphological properties of the synthesized CdS/MoS<sub>2</sub>/Bi<sub>2</sub>S<sub>3</sub> were explored. The effects of Bi<sub>2</sub>S<sub>3</sub> on CdS/MoS<sub>2</sub> were thoroughly studied by performing an X-ray diffractometer (XRD), a scanning electron microscope (SEM), an ultra-violet–visible spectrometer (Uv–vis), and Fourier transform infrared spectroscopic (FT-IR) studies of the nanoparticles. XRD confirms the cubical crystal structure of the nanoparticles. SEM studies possess the modulation in the surface morphology with the tenability in volume ratios of “MoS<sub>2</sub>/CdS/Bi<sub>2</sub>S<sub>3</sub>” composites. It was observed that the bandgaps calculated using absorption measurements could be manipulated from 2.40 eV to 0.97 eV with varying Bi<sub>2</sub>S<sub>3</sub> in the MoS<sub>2</sub>/CdS nanostructures. FT-IR confirmed the synthesis of “MoS<sub>2</sub>/CdS/Bi<sub>2</sub>S<sub>3</sub>” nanoparticles. On allowing the visible light to fall for 120 min, it was observed that “MoS<sub>2</sub>/CdS/Bi<sub>2</sub>S<sub>3</sub>” degrades the methylene blue up to 90%. The calculated results of “MoS<sub>2</sub>/CdS/Bi<sub>2</sub>S<sub>3</sub>” suggest that the synthesized material could be a strong candidate for photodegradation applications. This research work explains the synthesis of MoS<sub>2</sub>/CdS/Bi<sub>2</sub>S<sub>3</sub>-based nanocomposites for the degradation of dye using a photocatalytic process. The final results show that this catalyst effectively degrades the dye.

**Keywords:** CdS/MoS<sub>2</sub>/Bi<sub>2</sub>S<sub>3</sub>; photocatalysis; photodegradation; organic dye



**Citation:** Nazir, A.; Tahir, M.S.; Kamal, G.M.; Zhang, X.; Tahir, M.B.; Jiang, B.; Safdar, M. Fabrication of Ternary MoS<sub>2</sub>/CdS/Bi<sub>2</sub>S<sub>3</sub>-Based Nano Composites for Photocatalytic Dye Degradation. *Molecules* **2023**, *28*, 3167. <https://doi.org/10.3390/molecules28073167>

Academic Editors: Hem Raj Pant, Bishweshwar Pant and Deval Prasad Bhattarai

Received: 10 February 2023

Revised: 28 March 2023

Accepted: 31 March 2023

Published: 2 April 2023



**Copyright:** © 2023 by the authors. Licensee MDPI, Basel, Switzerland. This article is an open access article distributed under the terms and conditions of the Creative Commons Attribution (CC BY) license (<https://creativecommons.org/licenses/by/4.0/>).

## 1. Introduction

Water is necessary for many aspects of life, including growth and development. Safer and healthier drinking water is essential for maintaining public health [1]. Water is frequently used as one of the vital sources of life [2]. Water is a precious resource for many purposes, including domestic, industrial, and agricultural ones. It is also crucial for metabolic processes and cell function [3].

However, as the environment continues to deteriorate, there are various problems related to water pollution that also contaminate other parts of the ecosystem [4]. Furthermore, once polluted, the treatment of water is challenging and expensive, making it almost always impossible [5]. Water and water resources are essential for ensuring that all living species have access to enough food and a fertile habitat [6]. As the human population and economic activity have increased, so has the global need for freshwater [7]. Critical water resources are being placed under increasing pressure due to the adverse impacts of a growing global population, a changing climate, and different consumption habits, leading to widespread water stress in many countries [8]. Due to this, people are becoming more conscious of the urgent need to reduce their water use [9]. While developing nations face severe water pollution problems, industrialized nations still face pollution problems today [10]. Currently, 1.1 billion people are in danger because of a shortage of clean water, and 35% of fatal illnesses associated with water use occur in developing countries [11].

The development of technology has led to the introduction of several physical, chemical, and biological pollutants into the water supply. Wastewater includes liquid waste from houses, institutions, and industrial organizations. The pollution of waterways by industrial effluent is a global problem. There are high levels of several organic contaminants, heavy metals, and non-degradable compounds. Effectively eliminating these contaminants from industrial wastewater is of critical importance at present. Successful cleansing processes are required to eliminate these contaminants before they may be thrown away. Treatment methods for industrial wastewater may be divided into three broad categories: chemical, physical, and biological. The most often used technologies may be categorized as pre-treatments, primary treatments, secondary treatments, and tertiary treatments. Primary treatments, regularly used for essential cleaning, are size-based separations utilizing physical procedures similar to sedimentation and filtration. Secondary treatment can include physical, chemical, or biological methods to remove 80–90% of BOD, COD, and TSS from the wastewater. Tertiary treatment is used to further clean the effluent after secondary treatment by removing any harmful or dangerously recalcitrant pollutants (in some instances, this may be as high as 99%).

One of the methods available for efficiently treating wastewater is the use of nanomaterials. Water purification utilizing inexpensive nanoadsorbents and nanofiltration is an innovative use for nanomaterials. In this overview, we look at how nanoparticles are used to clean up industrial wastewater, emphasizing MB removal.

Industrial wastewater must be cleaned of organic dyes using practical, affordable methods that should be sustainable for the environment. The use of nanocomposite photocatalysts has been a very efficient way to treat industrial waste waters.

The use of photocatalysts is the most effective strategy for reducing organic dyes in manufacturing waste. The photocatalytic technique may be used to lessen environmental damage caused by industrial waste. CdS is one of the most promising photocatalysts for its nontoxicity, low cost, and photostability [9,10]. However, because of its large bandgap (2.42 eV), this frequently used CdS has poor photocatalytic effectiveness and is only photocatalytically active when exposed to UV light. Due to the smaller bandgap, visible-light photocatalysis was made possible [11]. However, several investigations have shown that CdS has weak photocatalytic activity. Metal-nonmetal doping is often used to create a defect level in the CdS band that is outlawed to optimize sunlight use [12,13].

The recombination impact of carriers further reduces the photocatalytic efficiency, yet a modest number of flaws are still virtually inadequate to improve the absorption of visible light radiation [14,15]. The reduced CdS (CdS-x) shows excellent visible light absorption and possesses a Cd<sup>2+</sup> or sulfur vacancy defect. Under xenon-light illumination, it was found that the rate of methylene blue (MB) deterioration was 2.7 times greater than that of pure CdS. CdS-x offers active sites in the prohibited bandgap and maintains the natural structure, in contrast to impurity incorporation.

Although the decreased CdS (CdS-x) had more flaws, substantial photoelectron and hole recombination continued to occur in single-phase CdS, resulting in poor photocatalytic

efficiency and hampering its use [16]. Heterostructures have been used to reduce carrier recombination by using semiconductor compounds, the deposition of noble metals, and the modification of carbon materials [17,18].

Nanoparticles are the most common sort of nanostructured material. According to the nanoscale model, nanoparticles are self-existent material units that are entirely isolated from one another by neighboring particles of a uniform size. They may also have a wide range of morphologies [17]. The creation of customized nanoparticles and their optimization for applications in various technological fields, including electronics, biomedicine, and catalysis, have received much attention during the last 20 years.

Nanoparticles fabricated from inorganic phases (metals, alloys, oxides, and composites) are typically preferred because of their enhanced electrical, optical, magnetic, and mechanical capabilities and the increased opportunities afforded by the smaller-than-nanometer-scale coupling between them [18]. Most industrial, environmental, and biological activities are based on aqueous chemistry, which is especially suitable for inorganic nanoparticles.

Furthermore, it has been suggested that nanoparticles could be used to filter out organic dyes from drinking water. Numerous early studies back up the idea that some particles may irreversibly remove one or more organic dyes and metals from industrial wastewater.

The thermal instability of these modified materials is causing a significant decline in photocatalytic activity [19,20]. Due to its thermal stability and capacity to offer catalytic activity,  $\text{MoS}_2/\text{Bi}_2\text{S}_3$  is a favored material. The photocatalytic characteristics of all the produced  $\text{CdS}/\text{MoS}_2/\text{Bi}_2\text{S}_3$  heterostructure photocatalysts are superior to those of pure  $\text{CdS}$  due to improved charge carrier separation efficiency [21,22].

Though, the synthesis technique of  $\text{CdS}/\text{MoS}_2$  composites is laborious, and the recycling process is challenging, still the material becomes more efficient by intimate contact of  $\text{MoS}_2$  on the surface of  $\text{CdS}$ . The photocatalytically active, micron-sized  $\text{CdS}/\text{MoS}_2$  composite photocatalysts are currently made using a three-step external source [23,24]. We proposed the loading of  $\text{Bi}_2\text{S}_3$  on the surface of  $\text{CdS}/\text{MoS}_2$  to synthesize a new composite with further enhanced photocatalytic activity. Through a unique hydrothermal process under embedded sintering conditions has been used in this study to manufacture an in-situ grey  $\text{CdS}/\text{MoS}_2/\text{Bi}_2\text{S}_3$  hetero-structure photocatalyst in a single step. Earlier research has revealed its ability to treat high, medium, and low turbidity water. It can also be used as a softening or dewatering agent, so its importance in wastewater treatment cannot be overstated.

When " $\text{CdS}/\text{MoS}_2/\text{Bi}_2\text{S}_3$ " is compared with conventional chemical coagulants, it has the following advantages: cost effectiveness, availability, biodegradable sludge, eco-friendliness, low sludge volume, it does not produce harmful by-products, it is easily handled as it is not corrosive, and it does not affect the pH of water. In the light of the above advantages, " $\text{CdS}/\text{MoS}_2/\text{Bi}_2\text{S}_3$ " is environmentally friendly and available at a low cost, which can be a good alternative to chemical photocatalysis with a potential application in wastewater treatment in industry. Therefore, using " $\text{CdS}/\text{MoS}_2/\text{Bi}_2\text{S}_3$ " as a photocatalyst in the industrial waste strategy to improve water quality will provide the best results.

## 2. Results and Discussion

It was possible to identify the crystal structure using an X-ray diffractometer. A scanning electron microscope (SEM) was used to analyze surface morphology. FT-IR confirms the synthesis of  $\text{MoS}_2/\text{CdS}/\text{Bi}_2\text{S}_3$  nanoparticles.

### 2.1. Morphological Studies

The nanoscale  $\text{MoS}_2$  particles are visible and successfully prepared composites of  $\text{MoS}_2$  nanostructure. The morphology of  $\text{MoS}_2/\text{CdS}$  was characterized using surface morphology as it was created. Figure 1a,b, respectively, show SEM images of  $\text{CdS}$  on  $\text{MoS}_2$ . The  $\text{CdS}$ , which resembled an olive, was shaped like a nanoflake's surface [25,26].

MoS<sub>2</sub> was connected irregularly to the edge of the CdS in the MoS<sub>2</sub>/CdS/Bi<sub>2</sub>S<sub>3</sub> composite, increasing the catalytic edge sites [27,28].

The brilliance of the orange colour in the MoS<sub>2</sub>/CdS composite decreased when the ratio of MoS<sub>2</sub>/Bi<sub>2</sub>S<sub>3</sub> increased. The surface-to-volume ratio of nanostructured materials makes assessing their surface highlights a must for several essential applications. Figure 1c shows the CdS/MoS<sub>2</sub>/Bi<sub>2</sub>S<sub>3</sub> composites (1%/1%/1%), the Figure 1d CdS/MoS<sub>2</sub>/Bi<sub>2</sub>S<sub>3</sub> composites (1%/0.5%/0.5%), the Figure 1e CdS/MoS<sub>2</sub>/Bi<sub>2</sub>S<sub>3</sub> composites (2%/5%/5%), and the Figure 1f CdS/MoS<sub>2</sub>/Bi<sub>2</sub>S<sub>3</sub> composites (0.1%/1%/1%). The particles of nano-sized CdS, MoS<sub>2</sub>, and Bi<sub>2</sub>S<sub>3</sub> are obviously clear, proposing a successful composite of CdS, MoS<sub>2</sub>, and Bi<sub>2</sub>S<sub>3</sub> nanostructures. SEM images of complete CdS/MoS<sub>2</sub>/Bi<sub>2</sub>S<sub>3</sub> nanoparticles demonstrate CdS/MoS<sub>2</sub>/Bi<sub>2</sub>S<sub>3</sub> nanoparticles.

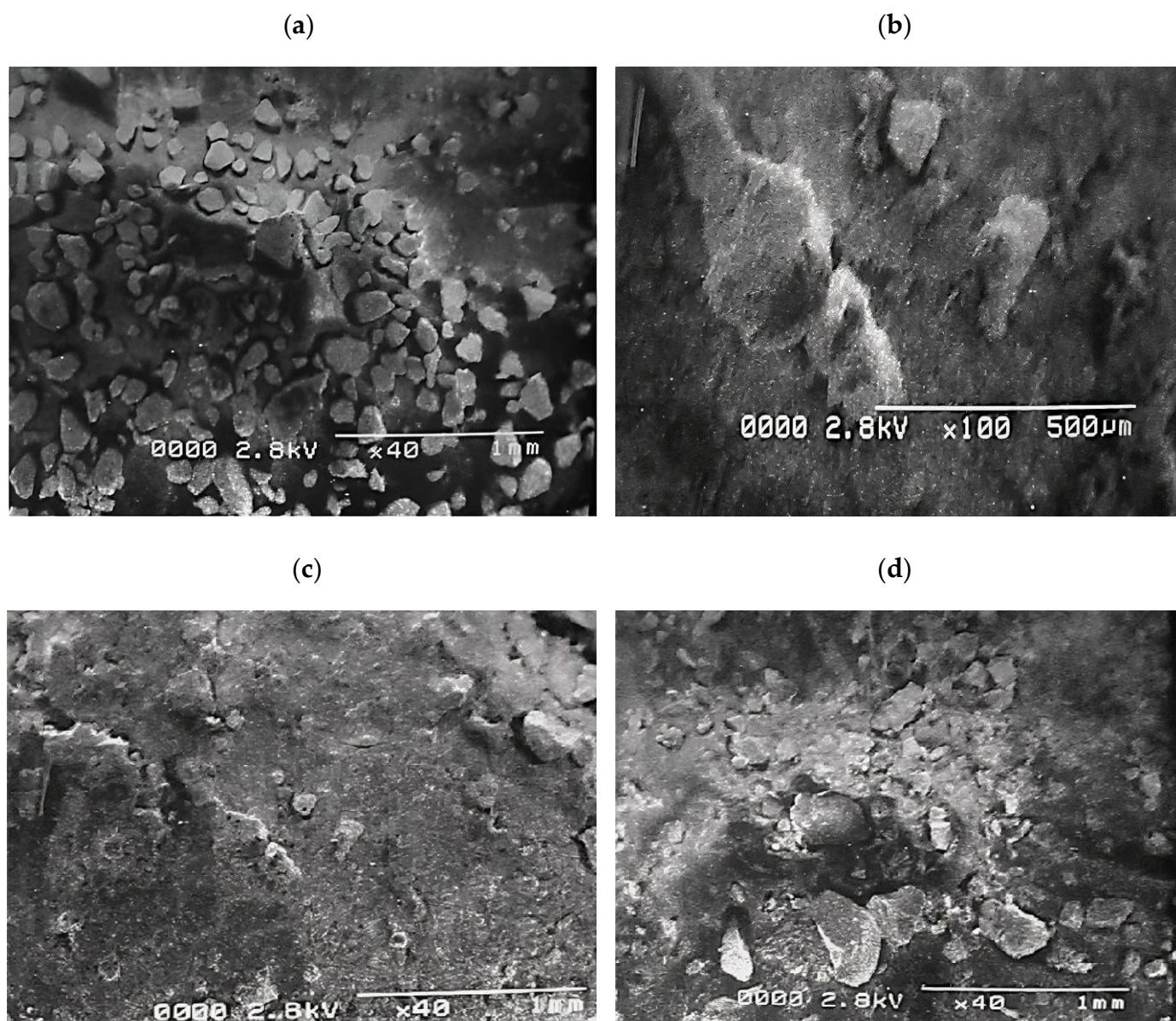
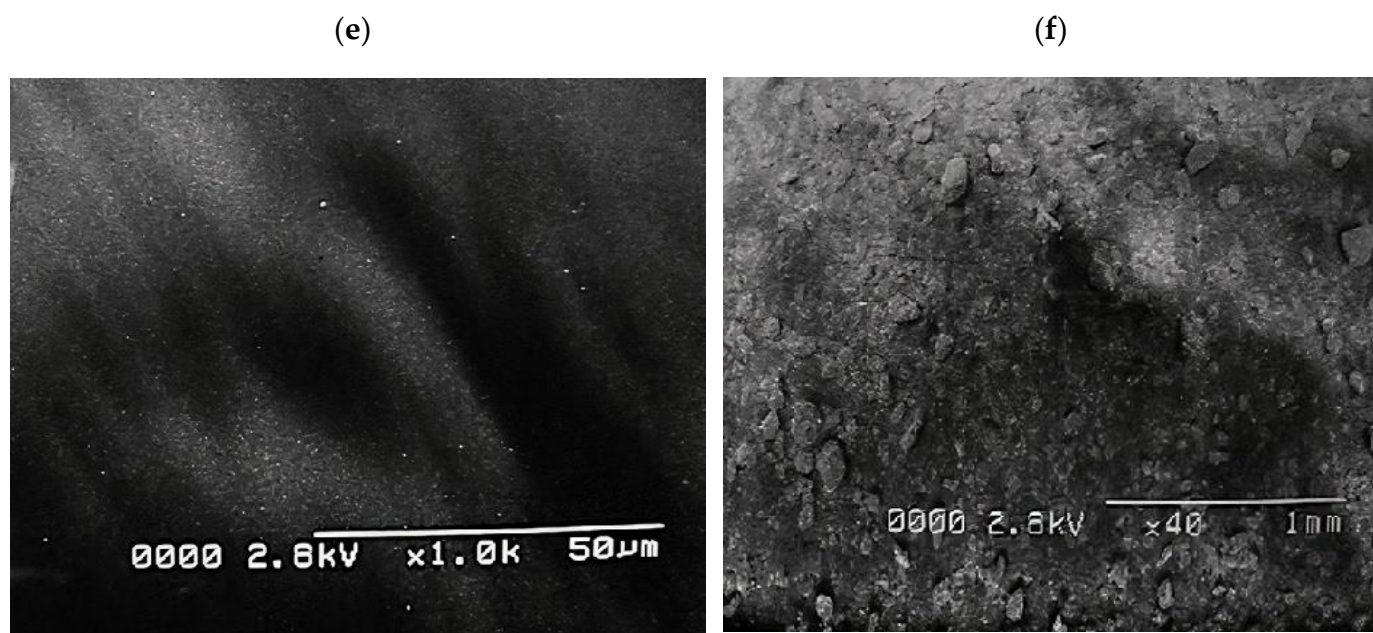


Figure 1. Cont.



**Figure 1.** (a) CdS, (b) MoS<sub>2</sub>, (c) CdS/MoS<sub>2</sub>/Bi<sub>2</sub>S<sub>3</sub> composites (1%/1%/1%), (d) CdS/MoS<sub>2</sub>/Bi<sub>2</sub>S<sub>3</sub> composites (1%/5%/5%), (e) CdS/MoS<sub>2</sub>/Bi<sub>2</sub>S<sub>3</sub> Composites (2%/5%/5%), and (f) CdS/MoS<sub>2</sub>/Bi<sub>2</sub>S<sub>3</sub> composites (0.1%/1%/1%).

## 2.2. Structural Studies

The overlapped FTIR spectra of the synthesized materials have been shown in Figure 2. The FTIR spectra cover an array of 4000 cm<sup>-1</sup> to 400 cm<sup>-1</sup>. The major peaks are at 3399 cm<sup>-1</sup>, 1624 cm<sup>-1</sup>, 1112 cm<sup>-1</sup>, and 418 cm<sup>-1</sup>. The extending style of the OH group, which is specified by water contents, is designated by an eclectic band at 3399 cm<sup>-1</sup>. The H-O-H bending vibrational mode is responsible for the band about 1624 cm<sup>-1</sup>, which is absorbed by water in the air. The FT-IR spectra of the precursor and product MoS<sub>2</sub>/CdS/Bi<sub>2</sub>S<sub>3</sub> nanocomposites are also shown in Figure 2. The I.R. bands at 428 cm<sup>-1</sup> and 508 cm<sup>-1</sup> are symptomatic of the stretching vibrations of the Mo-S and (S-S)<sub>2</sub> bonds [25,29].

Both the stretching vibration of the CdS link at 630 cm<sup>-1</sup> and the bending vibration of water at 1560 cm<sup>-1</sup> were both identified. Specifically, the prominent peak between 3200 and 3500 cm<sup>-1</sup> was associated with the O-H bond vibration [26]. This suggested that photoreduction, rather than adsorption, was the primary interaction mechanism on the MoS<sub>2</sub>/CdS composite, as no new bands appeared following the reaction [30,31].

The absorptions at 1627, 1427, 1112, 875, and 607 cm<sup>-1</sup> are all ascribed to MoS<sub>2</sub>, although the bands at 3000–2800 cm<sup>-1</sup> are produced by the stretching of the C-H alkyl stretching band in polyethylene glycol. Finally, FTIR concerns have long established the favorable implementation of MoS<sub>2</sub> nanocomposites [32].

We examined the FTIR range of the contrived MoS<sub>2</sub> nanoparticles and shown in Figure 2. Wide-ranging absorption bands were found at 639 cm<sup>-1</sup>, 893 cm<sup>-1</sup>, 1402 cm<sup>-1</sup>, and 1622 cm<sup>-1</sup> which are accredited to MoS<sub>2</sub>. The band at approximately 483 cm<sup>-1</sup> is due to the S-S bond. The 931 cm<sup>-1</sup> band is owed to the S-S bond. The peaks of about 3182 cm<sup>-1</sup> are distinguishing features of the O-H group [33,34].

Strong hydrogen bonding between the O-H bands at 3170 cm<sup>-1</sup> causes them to commonly overlap the C-H absorbance. CdS particles showed two C-O stretching bands at 997 cm<sup>-1</sup> and 653 cm<sup>-1</sup>, and CH<sub>3</sub> (acetone) bending, whether acute or wide, was papered at 1484 cm<sup>-1</sup>. Impurities such as SO<sub>4</sub> can be detected as a small absorption peak at 853 cm<sup>-1</sup>. The absorption at 2002–2926 cm<sup>-1</sup> is recognized as a stretching vibration of carbon and hydrogen.

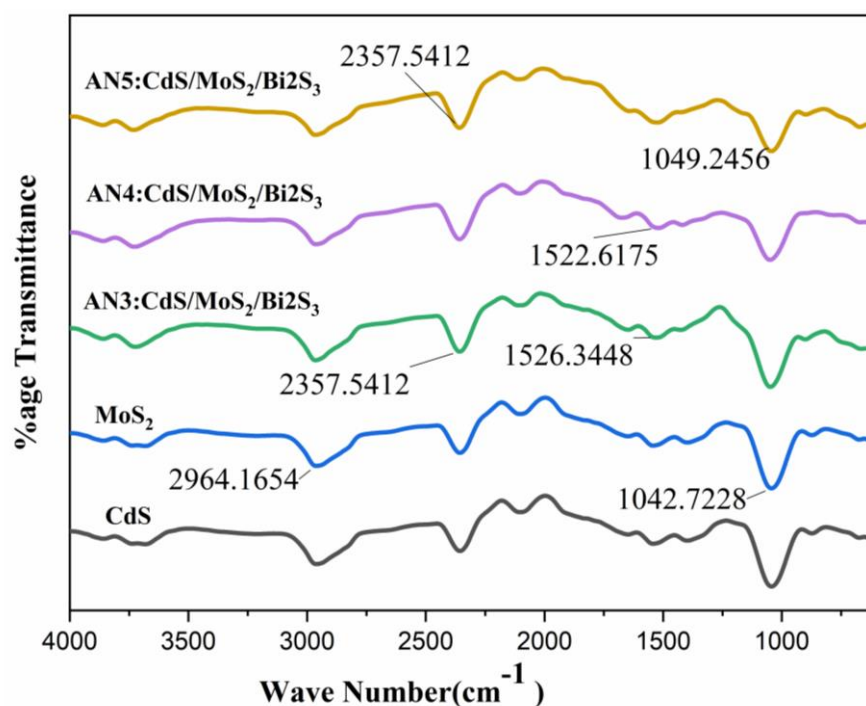


**Figure 2.** FTIR spectra of CdS, MoS<sub>2</sub>, (AN<sub>3</sub>)CdS/MoS<sub>2</sub>/Bi<sub>2</sub>S<sub>3</sub> composite (1%/1%/1%), (AN<sub>4</sub>)CdS/MoS<sub>2</sub>/Bi<sub>2</sub>S<sub>3</sub> composite (1%/5%/5%), and (AN<sub>5</sub>)CdS/MoS<sub>2</sub>/Bi<sub>2</sub>S<sub>3</sub> composite (2%/5%/5%).

Along with the peaks at 400–1000 cm<sup>-1</sup>, which are linked with Bi-S stretching vibration, an alternative peak seems to be at 1110 cm<sup>-1</sup>, which is accompanied by C–O, C=O, and C–S bending vibration.

### 2.3. XRD Analysis

Since atoms in different crystals release X-rays in different directions. Using an X-ray diffractometer (XRD JDX-3532 JEOL, Tokyo Japan), the crystallinity of as-prepared MoS<sub>2</sub>/CdS/Bi<sub>2</sub>S<sub>3</sub> was determined. A three-dimensional arrangement of electron density may be indomitable by evaluating the angles and scattering intensities of these beams. This technique may be used to determine crystal structure, chemical bonding, and other similar phenomena. Porous molybdenum disulfide's XRD pattern can be seen in Figure 3. Porous MoS<sub>2</sub> was effectively synthesized, as evidenced by peaks at 14.3° and weak peaks at 24.3° and 29.2°. (JCPDS card No. 37-1492).

Furthermore, the XRD spectrum of CdS nanoparticles is presented in Figure 3; peaks at 25.8, 43.2, and 51.3 °C agree with JCPDS 42-1411, representing the triumph for the production. Figure 3 also pertains to AN<sub>3</sub> (CdS/MoS<sub>2</sub>/Bi<sub>2</sub>S<sub>3</sub>) 1%1%/1% nanocomposites at 26.9°, 44.7°, and 52.5° [35]. Figure 3 also has to do with AN<sub>4</sub> (CdS/MoS<sub>2</sub>/Bi<sub>2</sub>S<sub>3</sub>, 1%:5%:5%) at 25.1°, 27.3°, and 46.1° to sanction the manifestation of the components Cd, S, and Mo in the manufactured nanoparticles and nanocomposites. The crystal configuration of MoS<sub>2</sub>/CdS was deliberated using XRD analysis [36]. The intense diffraction peak of the (101) plane shows that CdS crystals grew in that orientation. The diffraction peak intensity of MoS<sub>2</sub>/CdS was big and crisp, indicating excellent crystallization. The lack of a noticeable shift in the diffraction peak of MoS<sub>2</sub>/CdS composites when compared to CdS revealed that the loading of MoS<sub>2</sub> rather than doping was the cause. The lack of a diffraction peak in MoS<sub>2</sub> could be due to its low content [37]. After the photocatalytic reaction, the diffraction peaks did not significantly shift, indicating that the MoS<sub>2</sub>/Cd/Bi<sub>2</sub>S<sub>3</sub> composite was stable. It is acknowledged that high crystallinity is related to a reduction in crystal defects, which prevents the recombination of photogenerated electrons and holes and improves photocatalytic activity.

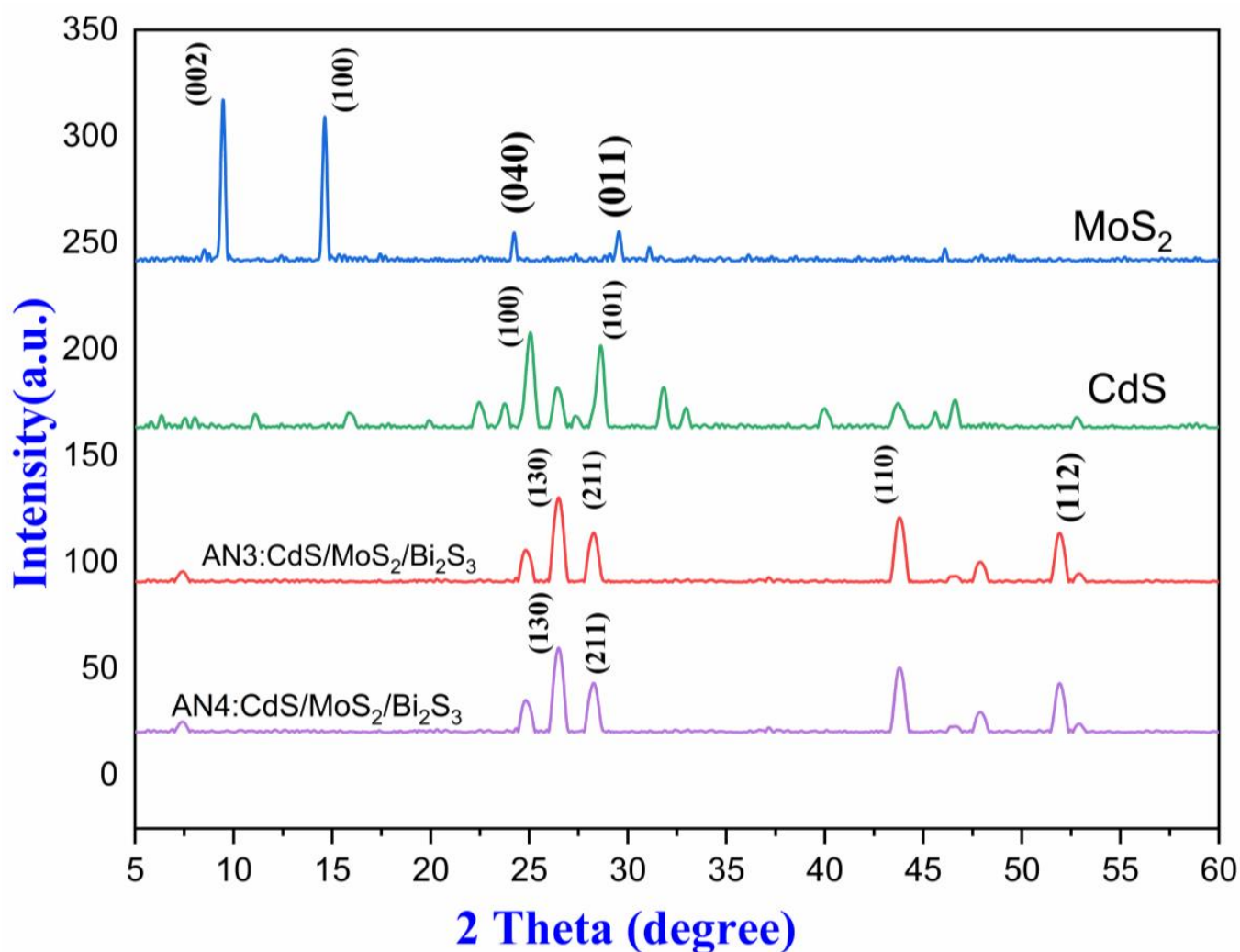


**Figure 3.** XRD spectra (CdS, AN3, AN4, and MoS<sub>2</sub>).

#### 2.4. UV-Vis Absorbance Spectra

The optical traits of MoS<sub>2</sub>/CdS nanocomposites were studied using UV-Vis and photocatalytic studies. UV-Vis spectra (for MoS<sub>2</sub>, CdS, and the MoS<sub>2</sub>/CdS nanocomposite) are presented in Figure 4. The UV-Vis absorption of MoS<sub>2</sub> is very weak, but when CdS is incorporated into MoS<sub>2</sub> to produce a MoS<sub>2</sub>/CdS nanocomposite, the absorption is enhanced and pushed down to shorter wavelengths. Studies in the UV-Vis range have been used to learn about the optical properties of MoS<sub>2</sub>/CdS nanocomposites. It is important to note that MoS<sub>2</sub> has weak UV-Vis absorption; however, that UV-Vis absorption is enhanced by a MoS<sub>2</sub>/CdS nanocomposite.

CdS nanoparticles, as shown in Figure 5a, feature a 3.4 eV bandgap and a maximum wavelength of 454 nm. The absorption spectra in Figure 4 show MoS<sub>2</sub>'s 1.6 eV bandgap [38]. Nanocomposites MoS<sub>2</sub>/CdS have a 2.8 eV bandgap, and their absorption spectra are shown in Figure 6 [36]. Due to the incorporation of MoS<sub>2</sub>, the bandgap energy was raised. The MoS<sub>2</sub>/CdS nanocomposite also exhibited an enhanced absorption curve in the visible spectrum.

The bandgap was found by using the following formula:

$$E_g = \frac{1240}{\lambda}$$

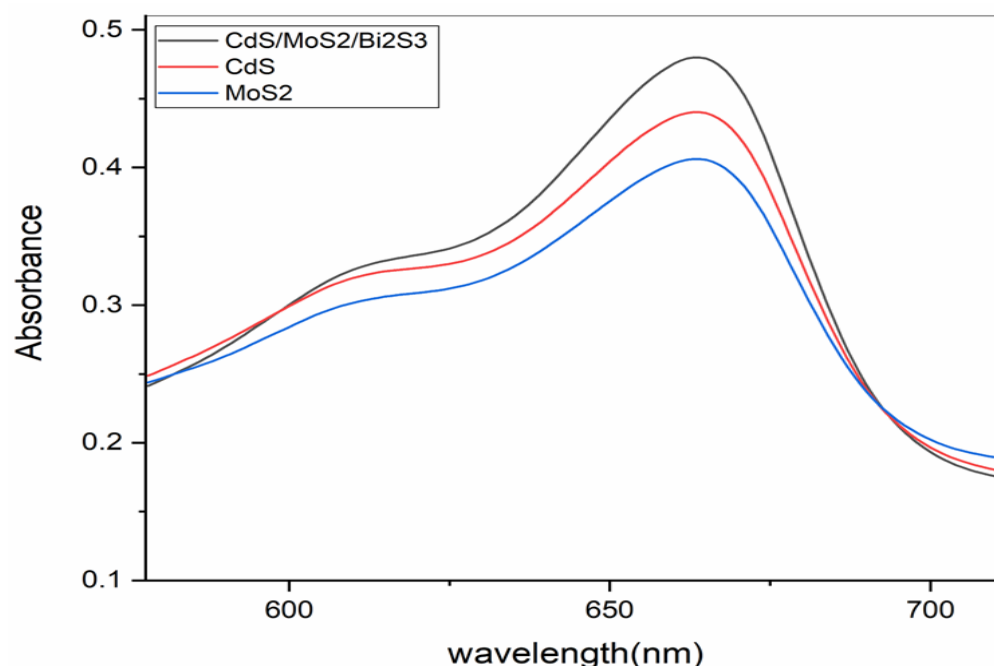


**Figure 4.** UV-Vis spectrum (CdS/MoS<sub>2</sub>/Bi<sub>2</sub>S<sub>3</sub>, CdS, and MoS<sub>2</sub>) before degradation.

#### 2.5. Photocatalytic Activity of CdS/MoS<sub>2</sub>/Bi<sub>2</sub>S<sub>3</sub>

When exposed to ultraviolet (UV) or visible light, the catalyst becomes active, producing free electrons and holes on its surface in addition to hydroxyl radicals. These free radicals oxidize and break down or eliminate organic pollutants. Reacting with the surface, oxygen is found naturally in the air, and water frees electrons trapped in the CdS. Due to its interaction with unstable oxygen free radicals, the O<sup>2-</sup> anion is formed, further oxidizing the organic molecules (superoxide).

CdS/MoS<sub>2</sub> is a useful photocatalyst because its surface undergoes many processes necessary for the degradation of organic dyes. The following formula was used to determine the effective photocatalytic degradation of organic dyes.

$$\text{photocatalytic degradation efficiency} = (C_0 - C/C_0) \times 100$$

where  $C_0$  is the dye solution concentration before photoirradiation, and  $C$  is the concentration of solutions in suspension after photoirradiation for a given time  $t$  [39,40].

To investigate the photocatalytic degradation of organic dyes like methylene blue, nanoparticles of CdS, MoS<sub>2</sub>, and Bi<sub>2</sub>S<sub>3</sub> were utilized. Figure 5 shows the typical degradation of methylene blue dye in the manifestation of CdS, MoS<sub>2</sub>, and Bi<sub>2</sub>S<sub>3</sub>, as well as the chemical and structural characteristics of the organic dyes used in this work [41]. Using lamps with wavelengths of 254 nm and 765 nm, ultraviolet light was used to expose the dyes. The Figures 7–9 show a typical measurement of organic dye absorbance vs. reaction time after exposure to a UV-Vis lamp with a longer wavelength of 670 nm. In methylene blue, the hetero-poly aromatic bond between the S and N atoms accounts for the high absorbance at 664 nm [42,43].

Due to  $n$  to  $\pi^*$  (the nitrogen atom has an unpaired electron pair) and to  $\pi^*$  (a system of double bonds that are conjugated in aromatic rings), absorbance peaks at 664 and 615 nm indicated that an electronic transition was occurring in the MB solution [21,22].

The value of MB solution absorbance in the absence of UV light and the CdS/MoS<sub>2</sub>/Bi<sub>2</sub>S<sub>3</sub> catalyst both dropped after 30 min, indicating that the CdS/MoS<sub>2</sub>/Bi<sub>2</sub>S<sub>3</sub> catalyst has a strong degrading capability. When CdS/MoS<sub>2</sub>/Bi<sub>2</sub>S<sub>3</sub> was utilized, the MB was completely damaged after 120 min of irradiation, but only 92% degraded after 100 min. Other researchers have reported comparable results using CdS/MoS<sub>2</sub>/Bi<sub>2</sub>S<sub>3</sub> for photocatalytic MB breakdown (Figures 7–9).

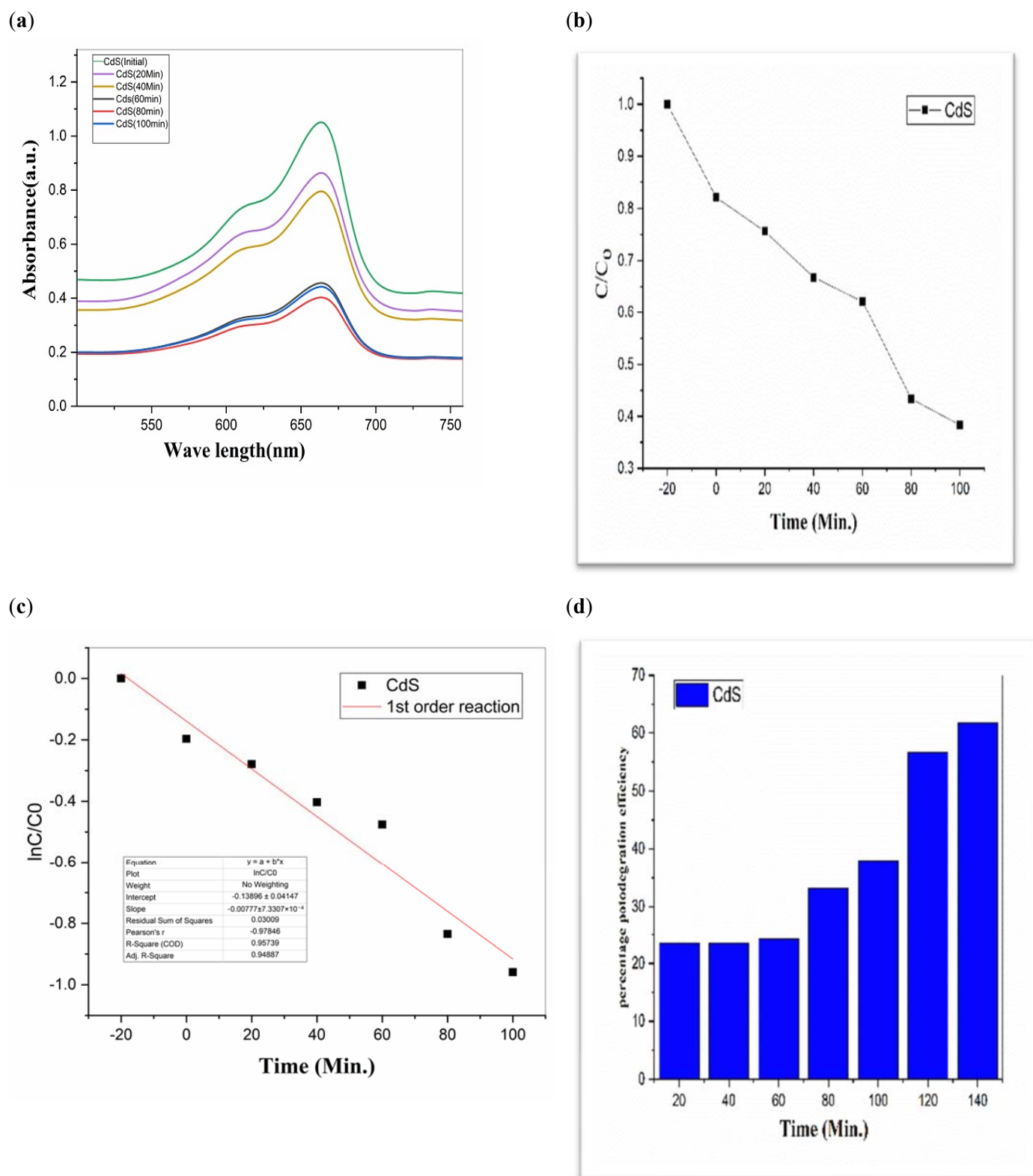


**Figure 5.** CdS (a) graphical representation of degradation of methylene blue; (b)  $C/C_0$ ; (c)  $\ln C/C_0$ ; (d) %age efficiency.

Although CdS/MoS<sub>2</sub>/Bi<sub>2</sub>S<sub>3</sub> particles had higher photocatalytic activity, the composite has nearly two times more dye absorption under similar conditions, indicating that the CdS/MoS<sub>2</sub>/Bi<sub>2</sub>S<sub>3</sub> phase had lower catalytic performance (Figures 7–9).

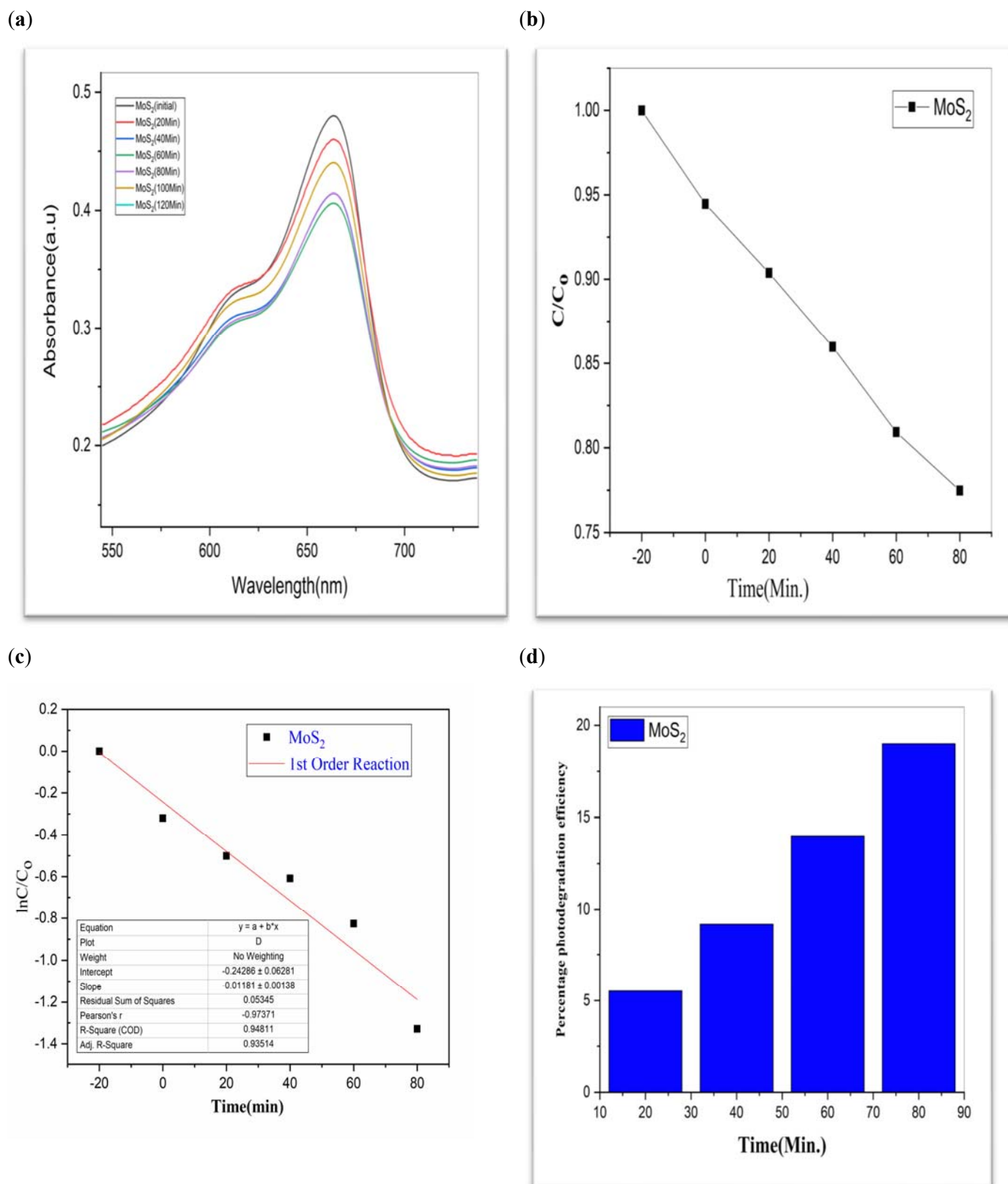


**Figure 6.** MoS<sub>2</sub> (a) graphical representation of degradation of methylene blue; (b)  $C/C_0$ ; (c)  $\ln C/C_0$ ; (d) %age efficiency.

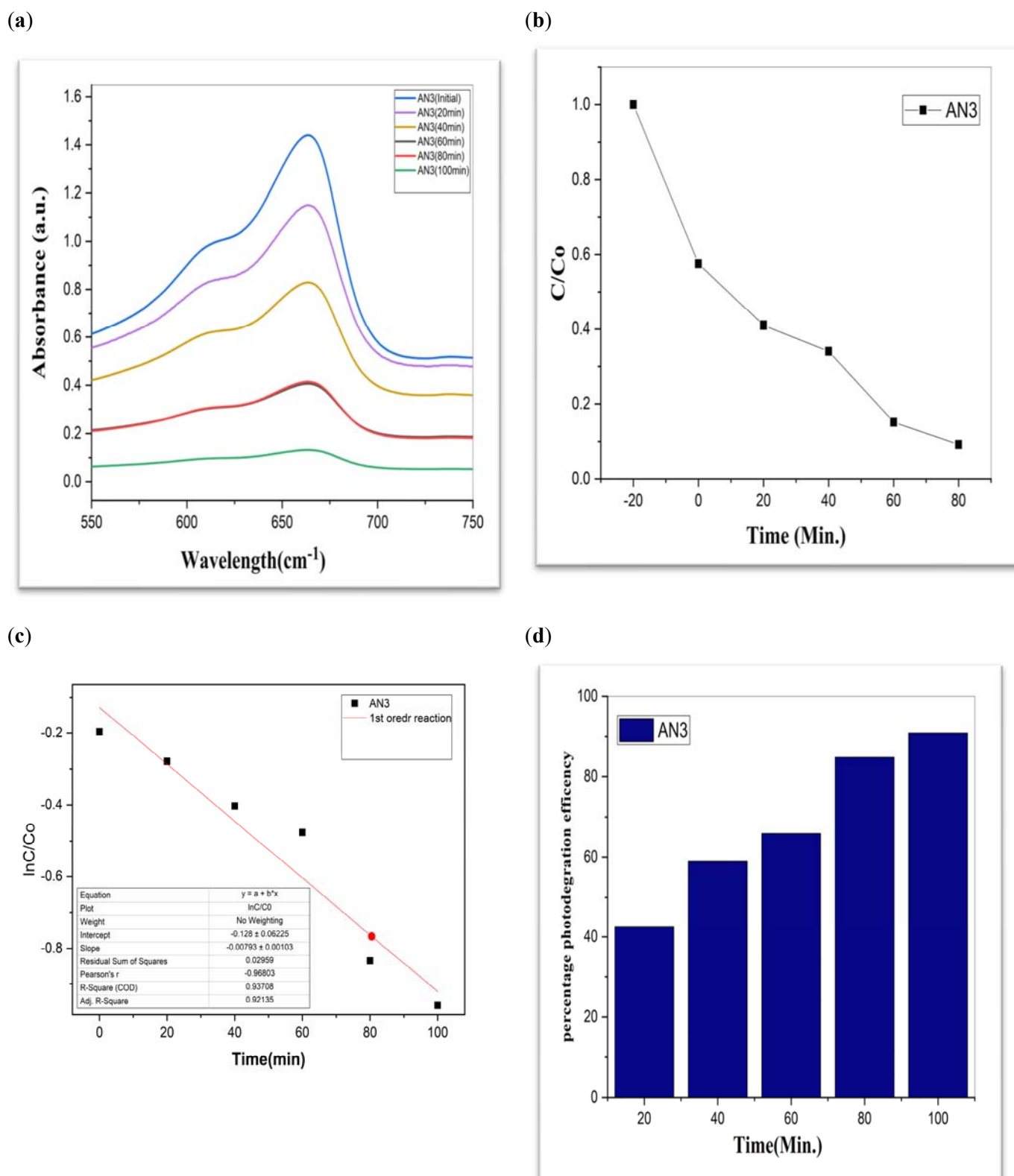


**Figure 7.** AN3 (a) graphical representation of degradation of methylene blue; (b)  $C/C_0$ ; (c)  $\ln C/C_0$ ; (d) %age efficiency.

Improved photocatalytic activity is anticipated from the anatase phase CdS/optimal  $\text{MoS}_2$ 's size quantization effect, which is the consequence of a larger surface area and a larger band gap as a result of smaller particles. Though MB degradation effectiveness was discovered to be 90% in the contemporary analysis, which might be connected to the

presence of more oxygen, as mentioned above, as well as smaller particle size obtained during CdS/MoS<sub>2</sub>/Bi<sub>2</sub>S<sub>3</sub> production.

It has been advocated that the low electron hole pair recombination rate of semiconductor nanoparticles is the most important factor in their efficient photocatalytic activity. Due to electronic excitation inside “CdS/MoS<sub>2</sub>/Bi<sub>2</sub>S<sub>3</sub>”, the photocatalytic process is kicked off when nanocomposite “CdS/MoS<sub>2</sub>/Bi<sub>2</sub>S<sub>3</sub>” is exposed to UV light.

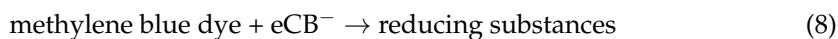
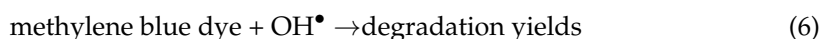
Direct activation of the nanoparticles is possible with energy superior to the bandgap of CdS, which is 3.2 eV (385 nm) [44,45]. According to numerous studies in the literature, the holes and electrons fashioned during photolysis can oxidize organic molecules, resulting in all of them being oxidized to •OH radicals when they interact with water or hydroxides. Photogenerated electrons may also enter the dye or combine with absorbed O<sub>2</sub> on nanoparticle planes to form the superoxide radical anion O<sub>2</sub><sup>•−</sup> [46].

The succeeding Equations (1)–(8) recapitulate the overall deterioration process as demonstrated graphically in Figure 10 [15].

So,

$$h\nu = \text{photons,}$$

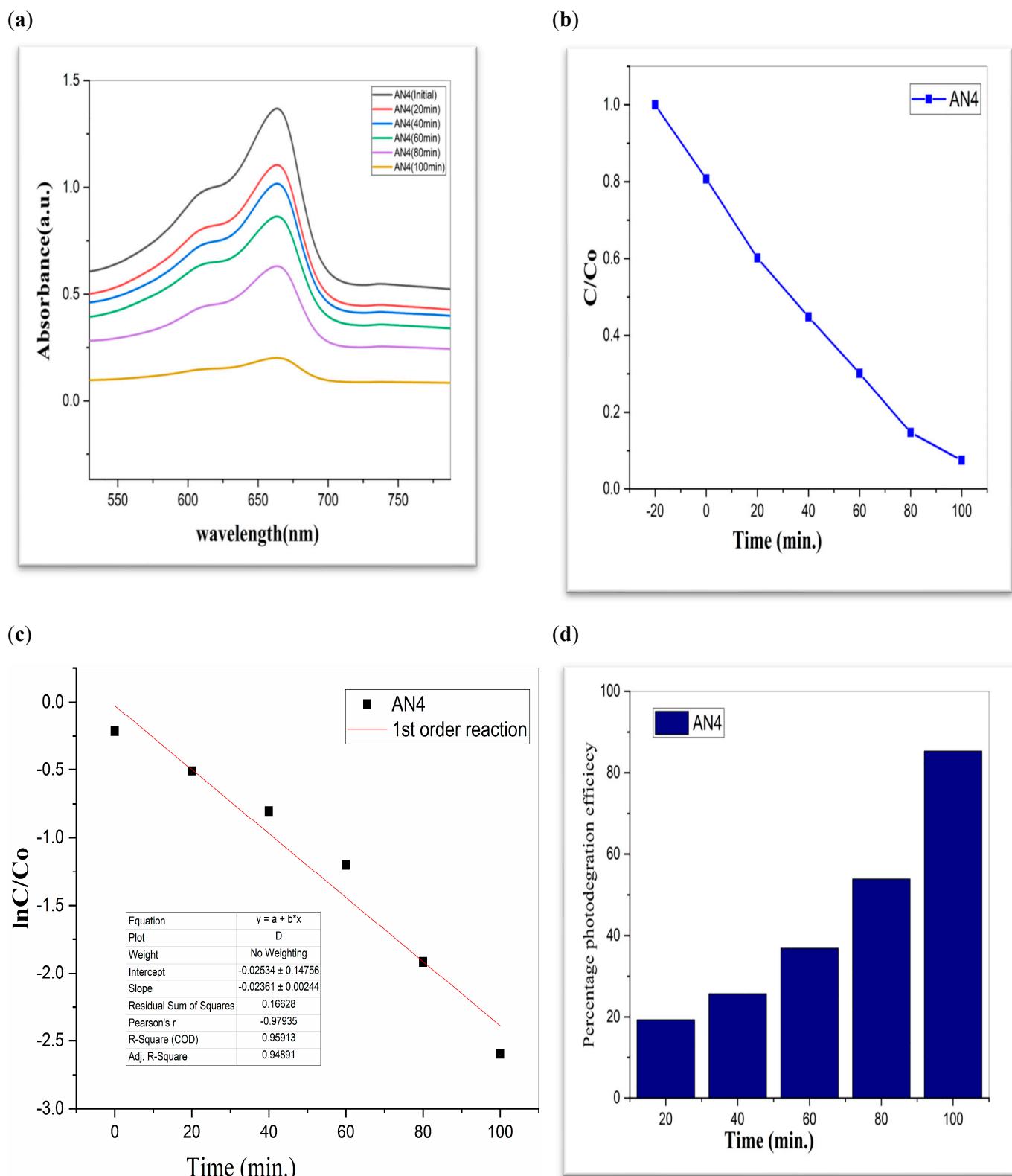
$$h = \text{holes and } e = \text{electrons}$$



examining methylene blue’s photocatalytic activity in its breakdown.

The photocatalytic activity of CdS/MoS<sub>2</sub>/Bi<sub>2</sub>S<sub>3</sub> nanoparticles for dye degradation was tested utilizing extended UV irradiation. The photocatalytic activity of “CdS/MoS<sub>2</sub>/Bi<sub>2</sub>S<sub>3</sub>” against MB is shown in the figure. The activity was set up to be appropriate in both conditions, though the degradation efficiency was found to be lower when associated with short UV irradiation. Other dyes were also studied to investigate the ability of composites to degrade them when exposed to UV light over longer periods of time the results of which will be published in our future research.

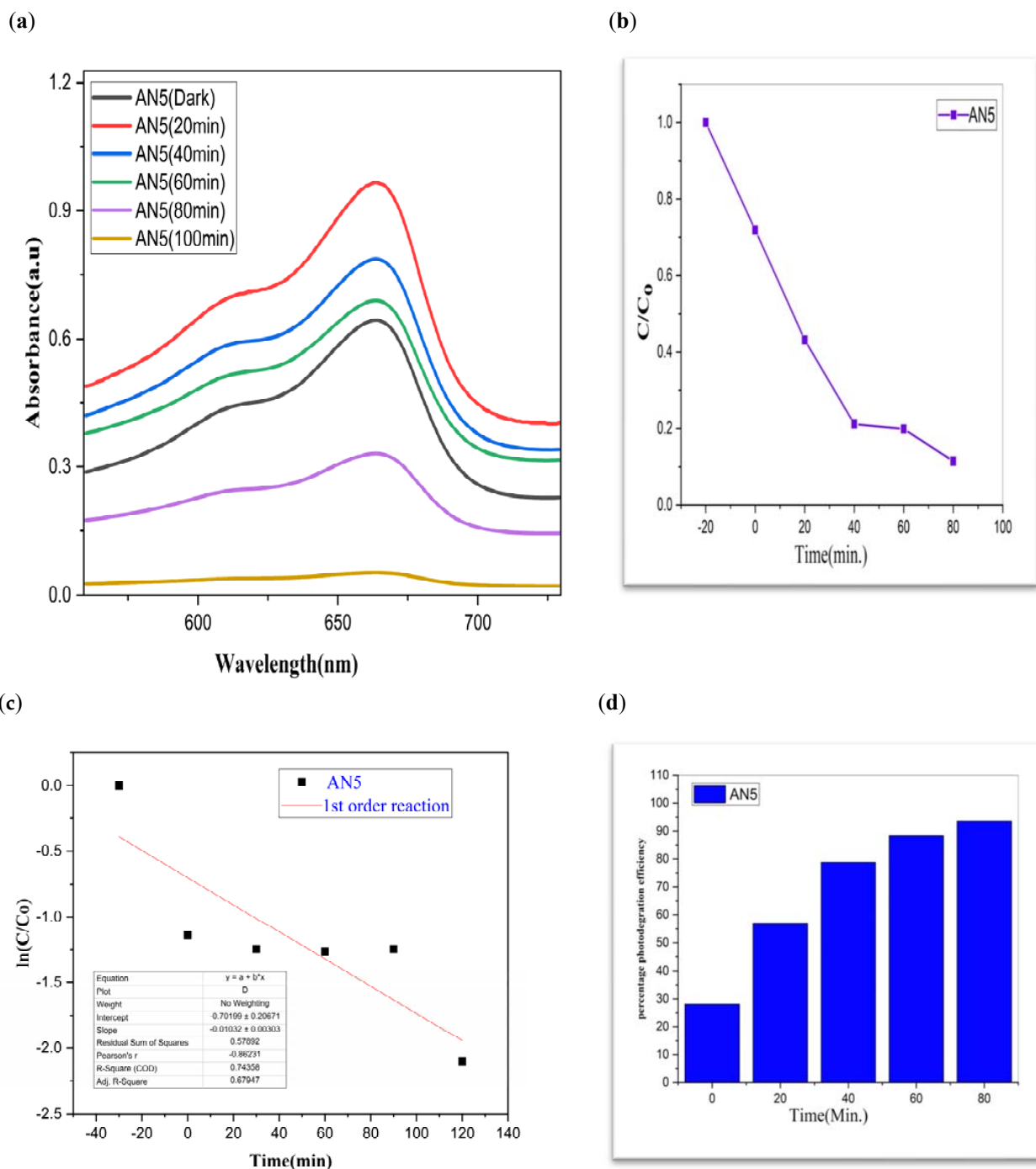
The graphs demonstrate the degradation of MB dye in the presence of CdS/MoS<sub>2</sub>/Bi<sub>2</sub>S<sub>3</sub>. Photocatalytic experiments with various compositions of nanocomposites demonstrated that the highest photocatalytic efficacy of about 90% was found to be for MB dye. Especially the photocatalytic degradation efficiency of “CdS/MoS<sub>2</sub>/Bi<sub>2</sub>S<sub>3</sub>” was found to be maximum i.e., 91% at ration of 2%:5%:5% (Table 1).



**Figure 8.** AN4 (a) graphical representation of degradation of methylene blue; (b)  $C/C_0$ ; (c)  $\ln C/C_0$ ; (d) %age efficiency.

**Table 1.** Degradation %age efficiency of synthesized materials.

Sr. No.	Composite	Percentage	Photodegradation Efficiency
1	MoS <sub>2</sub>	-	19%
2	CdS	-	65%
3	CdS/MoS <sub>2</sub> /Bi <sub>2</sub> S <sub>3</sub>	1:1:1	90%
4	CdS/MoS <sub>2</sub> /Bi <sub>2</sub> S <sub>3</sub>	1:5:5	88%
5	CdS/MoS <sub>2</sub> /Bi <sub>2</sub> S <sub>3</sub>	2:5:5	91%

**Figure 9.** AN5 (a) graphical representation of degradation of methylene blue; (b)  $C/C_0$ ; (c)  $\ln C/C_0$ ; (d) %age efficiency.

While comparing, CdS has a 60% efficiency in the photodegradation of MB, whereas MoS<sub>2</sub> only manages 19% (Table 1). But when we switched from Bi<sub>2</sub>S<sub>3</sub> to CdS/MoS<sub>2</sub>, we saw a 90% boost in efficiency. The optimal outcome was obtained using a composition of CdS, MoS<sub>2</sub>, and Bi<sub>2</sub>S<sub>3</sub>. The “CdS/MoS<sub>2</sub>/Bi<sub>2</sub>S<sub>3</sub>” performed the best i.e., 91% (Table 1).

We looked at the photocatalytic deterioration of MB in the presence of visible light. Different molar ratios in “CdS/MoS<sub>2</sub>/Bi<sub>2</sub>S<sub>3</sub>” samples showed more significant photocatalytic activity when compared to dark blue “CdS/MoS<sub>2</sub>/Bi<sub>2</sub>S<sub>3</sub>”. The enhanced photocatalytic performance of “CdS/MoS<sub>2</sub>/Bi<sub>2</sub>S<sub>3</sub>” composite photocatalysts was also found. The “CdS/MoS<sub>2</sub>/Bi<sub>2</sub>S<sub>3</sub>” samples with microstructure also have a lot of potential applications in water treatment.

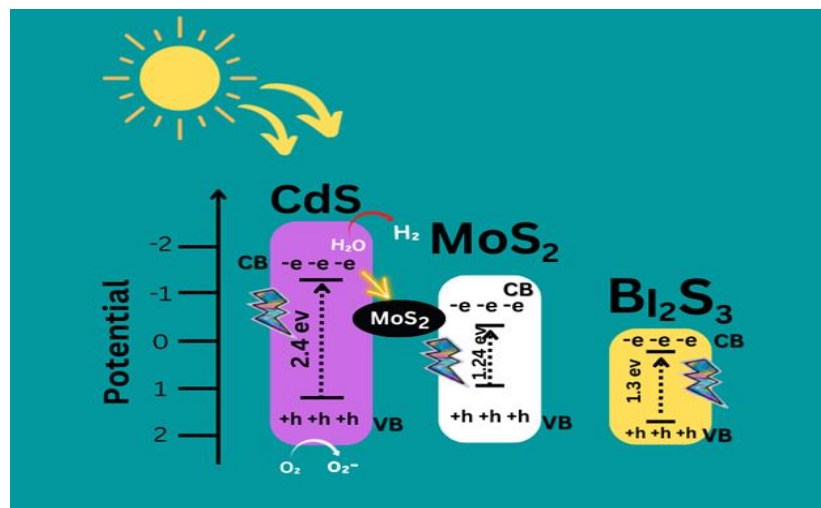


Figure 10. Proposed Mechanism of CdS/MoS<sub>2</sub>/Bi<sub>2</sub>S<sub>3</sub>.

### 3. Materials and Methods

#### 3.1. Synthesis of MoS<sub>2</sub> Photocatalyst

The graphical representation of the synthesis of photocatalyst composites has been shown in Figure 11. A 0.92 g sample of ammonium heptamolybdate tetrahydrate was diluted in 50 mL of ethylene glycol. Then, it was continuously mixed with 5 mL of hydrazine for 30 min. The mixture was then heated to 200 °C for 24 h while enclosed in a hydrothermal reactor coated with Teflon. After the reaction was complete, the container was allowed to cool at room temperature, and distilled water was used to wash the product. After multiple washes in ethanol, the resulting material was placed into a heated oven at 60 °C for 24 h in order to dehydrate. The product was allowed to cool at room temperature until further characterization and photocatalytic investigation.

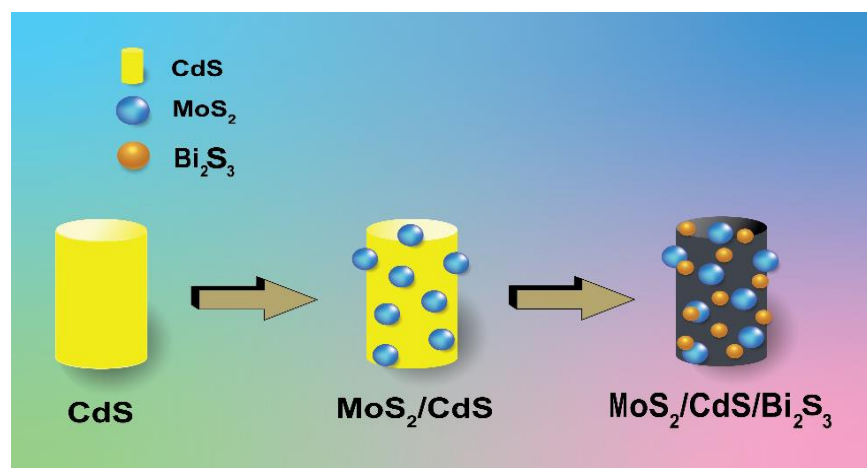


Figure 11. Product of CdS/MoS<sub>2</sub>/Bi<sub>2</sub>S<sub>3</sub>.

### 3.2. Synthesis of CdS Photocatalyst

In the first step, 3.085 g of “ $\text{Cd}(\text{NO}_3)_2 \cdot 4\text{H}_2\text{O}$ ” cadmium nitrate tetrahydrate was dissolved in 25 mL of distilled water. After that, 1.565 g of “ $\text{Na}_2\text{S}$ ” and 0.316 g of “ $\text{Na}_2\text{SO}_3$ ” were added to the aqueous solution of cadmium nitrate tetrahydrate. A 5 mL solution of acetic acid, 20 mL of ethylene glycol, and 1 g of “ $\text{Na}_2\text{EDTA}$ ” were then added with constant stirring for 30 min. Furthermore, the solutions were mixed well in a stainless-steel autoclave lined with Teflon, which was then sonicated for an hour. After that, the autoclave was cooked in an air-blowing thermostatic oven at 180 °C for six hours. The residue was dried in a vacuum chamber at room temperature overnight, followed by washing with ethanol and water.

### 3.3. Synthesis of CdS/MoS<sub>2</sub>/Bi<sub>2</sub>S<sub>3</sub> Composites

To obtain the wanted solution, we took 0.5 g of ascorbic acid dissolved in distillation water, added 0.5 g of MoS<sub>2</sub>, 0.5 g of CdS, 0.485 g of Bi(NO<sub>3</sub>)<sub>3</sub>·5H<sub>2</sub>O as a source of Bi, and 0.1126 g of thioacetamide as a source of sulfur, followed by 1 mL of ethylene diamine and 30 min of stirring (Figure 12). This solution was sonicated for 1 h after being well mixed in a Teflon-lined stainless steel autoclave. The autoclave, formed of stainless steel and layered with Teflon material, was placed in a thermostatic oven that heated the air to 200 °C for 24 h. After being washed in ethanol and water, the residue was dried in a vacuum compartment at room temperature for 12 h. We synthesized three different composites by varying the ratios of CdS, MoS<sub>2</sub>, and Bi<sub>2</sub>S<sub>3</sub>. The synthesized composites with specific ratios were as follows: AN3 with a ratio of 1:1:1; AN4 with a ratio of 1%/5%/5%; and AN5 with a ratio of 2%/5%/5% of CdS, MoS<sub>2</sub>, and Bi<sub>2</sub>S<sub>3</sub>, respectively.

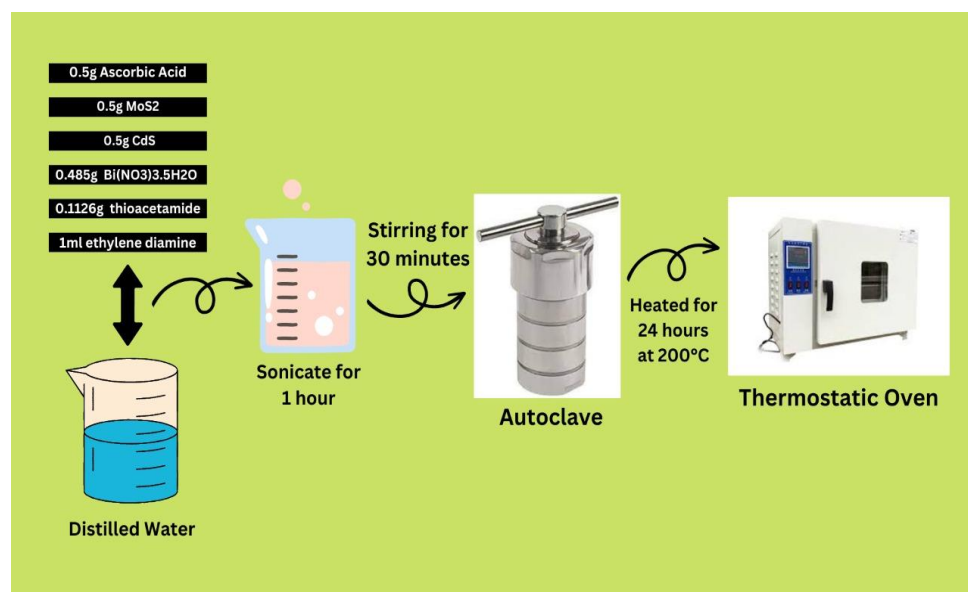


Figure 12. Synthesis of CdS/MoS<sub>2</sub>/Bi<sub>2</sub>S<sub>3</sub> composites.

## 4. Conclusions

We have successfully made “CdS/MoS<sub>2</sub>/Bi<sub>2</sub>S<sub>3</sub>” nano hybrids with different structures and looked at their photodegradation processes. The 3D designs of “CdS/MoS<sub>2</sub>/Bi<sub>2</sub>S<sub>3</sub>” nano hybrids displayed unusual sunlight-induced photocatalytic activities for decomposing three organic compounds. In sunlight irradiation, the “CdS/MoS<sub>2</sub>/Bi<sub>2</sub>S<sub>3</sub>” nano heterojunctions found extraordinarily high photodegradation efficiencies, resulting in the breakdown of 90.3% of the MB dye within 120 min. Superior photodegradation activity has been attained because of the synergistic effect’s high density between “CdS/MoS<sub>2</sub>” and Bi<sub>2</sub>S<sub>3</sub>. This effectively reduces the recombination rate and increases the charge separation process. Significant data demonstrate how varied “CdS/MoS<sub>2</sub>/Bi<sub>2</sub>S<sub>3</sub>” nano hybrid morphologies

impact the heterojunction density. This work emphasizes the straightforward method for creating “CdS/MoS<sub>2</sub>/Bi<sub>2</sub>S<sub>3</sub>” heterojunctions for the outstanding photodegradation of organic azo dyes and pharmaceutical waste driven by sunlight. It can be shown that the cost-effective “CdS/MoS<sub>2</sub>/Bi<sub>2</sub>S<sub>3</sub>” nano hybrids are particularly useful for several industrial applications, including H<sub>2</sub> production, solar cells, and water splitting.

**Author Contributions:** Conceptualization, M.S.T.; methodology, G.M.K.; software, M.B.T.; validation, M.S.; formal analysis, X.Z.; funding, B.J.; data curation, A.N.; writing—original draft preparation, A.N.; visualization, M.S.T.; supervision, G.M.K.; project administration, M.S.T.; funding acquisition, X.Z. All authors have read and agreed to the published version of the manuscript.

**Funding:** This research was funded by the National Natural Science Foundation of China at the Chinese Academy of Science, and the APC was funded by Grant numbers 21974149 and 22174152.

**Institutional Review Board Statement:** Not applicable.

**Informed Consent Statement:** Not applicable.

**Data Availability Statement:** The data will be available on request.

**Conflicts of Interest:** The authors declare no conflict of interest.

**Sample Availability:** Samples of the compounds are available from the authors.

## References

1. Hollaway, M.J.; Beven, K.J.; Benskin, C.M.H.; Collins, A.; Evans, R.; Falloon, P.; Forber, K.J.; Hiscock, K.M.; Kahana, R.; Macleod, C.J.A. The challenges of modelling phosphorus in a headwater catchment: Applying a ‘limits of acceptability’ uncertainty framework to a water quality model. *J. Hydrol.* **2018**, *558*, 607–624. [[CrossRef](#)]
2. Shah, V.D. *Fluid Thoughts-Water: Structure and Mysticism*; Notion Press: Chennai, India, 2017.
3. Ashfaq, A.; Clochard, M.-C.; Coqueret, X.; Dispenza, C.; Driscoll, M.S.; Ulański, P.; Al-Sheikhly, M.J.P. Polymerization reactions and modifications of polymers by ionizing radiation. *Polymers* **2020**, *12*, 2877. [[CrossRef](#)] [[PubMed](#)]
4. Boretti, A.; Rosa, L. Reassessing the projections of the world water development report. *NPJ Clean Water* **2019**, *2*, 15. [[CrossRef](#)]
5. Pereira, L. Seaweeds as source of bioactive substances and skin care therapy—cosmeceuticals, algotherapy, and thalassotherapy. *Cosmetics* **2018**, *5*, 68. [[CrossRef](#)]
6. Hirschon, R. Essential Objects and the Sacred: Interior and Exterior Space in an Urban Greek Locality 1. In *Women and Space*; Routledge: Oxford, UK, 2021; pp. 70–86.
7. Salgot, M.; Folch, M. Wastewater treatment and water reuse. *Curr. Opin. Environ. Sci. Health* **2018**, *2*, 64–74. [[CrossRef](#)]
8. Saleh, H.M.; Hassan, A.I. Water chemistry in the biological studies by using nuclear analytical techniques. In *Water Engineering Modeling and Mathematic Tools*; Elsevier: Amsterdam, The Netherlands, 2021; pp. 133–156.
9. Tan, L.; Dong, W.; Liu, K.; Luo, T.; Gu, X. Thermal decomposition in-situ preparation of gray rutile TiO<sub>2-x</sub>/Al<sub>2</sub>O<sub>3</sub> composite and its enhanced visible-light-driven photocatalytic properties. *Opt. Mater.* **2021**, *111*, 110716. [[CrossRef](#)]
10. Lewis, N.S. Research opportunities to advance solar energy utilization. *Science* **2016**, *351*, aad1920. [[CrossRef](#)] [[PubMed](#)]
11. Sohn, Y.; Huang, W.; Taghipour, F. Recent progress and perspectives in the photocatalytic CO<sub>2</sub> reduction of Ti-oxide-based nanomaterials. *Appl. Surf. Sci.* **2017**, *396*, 1696–1711. [[CrossRef](#)]
12. Dong, W.; Liu, H.; Bao, Q.; Gu, X. Facile synthesis of metastable CaTi<sub>2</sub>O<sub>5</sub> nanostructure and its photocatalytic properties. *Opt. Mater.* **2020**, *105*, 109921. [[CrossRef](#)]
13. Wang, Z.; Li, C.; Domen, K. Recent developments in heterogeneous photocatalysts for solar-driven overall water splitting. *Chem. Soc. Rev.* **2019**, *48*, 2109–2125. [[CrossRef](#)]
14. Matos, J.; Ocares-Riquelme, J.; Poon, P.S.; Montaña, R.; García, X.; Campos, K.; Hernández-Garrido, J.C.; Titirici, M.M. C-doped anatase TiO<sub>2</sub>: Adsorption kinetics and photocatalytic degradation of methylene blue and phenol, and correlations with DFT estimations. *J. Colloid Interface Sci.* **2019**, *547*, 14–29. [[CrossRef](#)]
15. Qi, S.; Zhang, K.; Zhang, Y.; Zhang, R.; Xu, H. TiO<sub>2</sub>/Zn<sub>0.5</sub>Cd<sub>0.5</sub>S heterojunction for efficient photocatalytic degradation of methylene blue and its photocatalytic mechanism. *Chem. Phys. Lett.* **2022**, *798*, 139614. [[CrossRef](#)]
16. Karthikeyan, K.; Chandraprabha, M.; Krishna, R.H.; Samrat, K.; Sakunthala, A.; Sasikumar, M. Optical and antibacterial activity of biogenic core-shell ZnO@TiO<sub>2</sub> nanoparticles. *J. Indian Chem. Soc.* **2022**, *99*, 100361. [[CrossRef](#)]
17. Peng, Y.; Zhou, H.; Wu, Y.; Ma, Z.; Zhang, R.; Tu, H.; Jiang, L. A new strategy to construct cellulose-chitosan films supporting Ag/Ag<sub>2</sub>O/ZnO heterostructures for high photocatalytic and antibacterial performance. *J. Colloid Interface Sci.* **2022**, *609*, 188–199. [[CrossRef](#)]
18. Tahir, M.B.; Nabi, G.; Khalid, N.R. Enhanced photocatalytic performance of visible-light active graphene-WO<sub>3</sub> nanostructures for hydrogen production. *Mater. Sci. Semicond. Process.* **2018**, *84*, 36–41. [[CrossRef](#)]

19. Bilal Tahir, M.; Nabi, G.; Rafique, M.; Khalid, N.R. Role of fullerene to improve the WO<sub>3</sub> performance for photocatalytic applications and hydrogen evolution. *Int. J. Energy Res.* **2018**, *42*, 4783–4789. [[CrossRef](#)]
20. Luo, J.; Li, R.; Chen, Y.; Zhou, X.; Ning, X.; Zhan, L.; Ma, L.; Xu, X.; Xu, L.; Zhang, L.J.S.; et al. Rational design of Z-scheme LaFeO<sub>3</sub>/SnS<sub>2</sub> hybrid with boosted visible light photocatalytic activity towards tetracycline degradation. *Sep. Purif. Technol.* **2019**, *210*, 417–430. [[CrossRef](#)]
21. Adeleke, J.; Theivasanthi, T.; Thiruppathi, M.; Swaminathan, M.; Akomolafe, T.; Alabi, A.B. Photocatalytic degradation of methylene blue by ZnO/NiFe<sub>2</sub>O<sub>4</sub> nanoparticles. *Appl. Surf. Sci.* **2018**, *455*, 195–200. [[CrossRef](#)]
22. Hamad, H.N.; Idrus, S. Recent Developments in the Application of Bio-Waste-Derived Adsorbents for the Removal of Methylene Blue from Wastewater: A Review. *Polymers* **2022**, *14*, 783. [[CrossRef](#)]
23. Liu, J.; Liu, Y.; Liu, N.; Han, Y.; Zhang, X.; Huang, H.; Lifshitz, Y.; Lee, S.-T.; Zhong, J.; Kang, Z. Metal-free efficient photocatalyst for stable visible water splitting via a two-electron pathway. *Science* **2015**, *347*, 970–974. [[CrossRef](#)]
24. Xu, J.; Cao, X. Characterization and mechanism of MoS<sub>2</sub>/CdS composite photocatalyst used for hydrogen production from water splitting under visible light. *Chem. Eng. J.* **2015**, *260*, 642–648. [[CrossRef](#)]
25. Sun, Y.; Xiao, J.; Huang, X.; Mei, P.; Wang, H.; Research, P. Boosting photocatalytic efficiency of MoS<sub>2</sub>/CdS by modulating morphology. *Environ. Sci. Pollut. Res.* **2022**, *29*, 73282–73291. [[CrossRef](#)] [[PubMed](#)]
26. Shi, J.; Yang, L.; Zhang, J.; Wang, Z.; Zhu, W.; Wang, Y.; Zou, Z. Dual MOF-Derived MoS<sub>2</sub>/CdS Photocatalysts with Rich Sulfur Vacancies for Efficient Hydrogen Evolution Reaction. *Chem. A Eur. J.* **2022**, *28*, e202202019. [[CrossRef](#)] [[PubMed](#)]
27. Zhao, H.; Fu, H.; Yang, X.; Xiong, S.; Han, D.; An, X. MoS<sub>2</sub>/CdS rod-like nanocomposites as high-performance visible light photocatalyst for water splitting photocatalytic hydrogen production. *Int. J. Hydrogen Energy* **2022**, *47*, 8247–8260. [[CrossRef](#)]
28. Liu, X.; Wang, B.; Heng, Q.; Chen, W.; Li, X.; Mao, L.; Shanguan, W. Promoted charge separation on 3D interconnected Ti<sub>3</sub>C<sub>2</sub>/MoS<sub>2</sub>/CdS composite for enhanced photocatalytic H<sub>2</sub> production. *Int. J. Hydrogen Energy* **2022**, *47*, 8284–8293. [[CrossRef](#)]
29. Zheng, X.; Han, H.; Liu, J.; Yang, Y.; Pan, L.; Zhang, S.; Meng, S.; Chen, S. Sulfur Vacancy-Mediated Electron–Hole Separation at MoS<sub>2</sub>/CdS Heterojunctions for Boosting Photocatalytic N<sub>2</sub> Reduction. *ACS Appl. Energy Mater.* **2022**, *5*, 4475–4485. [[CrossRef](#)]
30. Yue, Y.; Shen, S.; Cheng, W.; Han, G.; Wu, Q.; Jiang, J.J.C.; Physicochemical, S.A.; Aspects, E. Construction of mechanically robust and recyclable photocatalytic hydrogel based on nanocellulose-supported CdS/MoS<sub>2</sub>/Montmorillonite hybrid for antibiotic degradation. *Colloids Surf. A Physicochem. Eng. Asp.* **2022**, *636*, 128035. [[CrossRef](#)]
31. Allahyar, S.; Taheri, M.; Allahyar, S. Facile synthesis of few-Layered MoS<sub>2</sub> Nanoroses Covering TiO<sub>2</sub> Nanowires as improved bacterial inactivation and photodegradation devices. *Res. Sq.* **2023**. [[CrossRef](#)]
32. Liu, Y.; Gong, L.; Zhang, Y.; Wang, P.; Wang, G.; Bai, F.; Zhao, Z.; Gong, F.; Liu, J. Metal Sulfides Yolk–Shell Nanoreactors with Dual Component for Enhanced Acidic Electrochemical Hydrogen Production. *Small Struct.* **2022**, *4*, 2200247. [[CrossRef](#)]
33. Qin, Y.; Xiao, K.; Sun, S.; Wang, Y.; Kang, C. Fabrication of a novel pyramidal 3D MoS<sub>2</sub>/2D PbTiO<sub>3</sub> nanocomposites and the efficient photocatalytic removal of organic pollutants: Effects of the PbTiO<sub>3</sub> internal electric field and S-scheme heterojunction formation. *Appl. Surf. Sci.* **2023**, *615*, 156431. [[CrossRef](#)]
34. Han, C.; Cheng, C.; Liu, F.; Li, X.; Wang, G.; Li, J. Preparation of CdS–Ag<sub>2</sub>S nanocomposites by ultrasound-assisted UV photolysis treatment and its visible light photocatalysis activity. *Nanotechnol. Rev.* **2023**, *12*, 20220503. [[CrossRef](#)]
35. Park, Y.H.; Kim, D.; Hiragond, C.B.; Lee, J.; Jung, J.-W.; Cho, C.-H.; In, I.; In, S.-I. Phase-controlled 1T/2H-MoS<sub>2</sub> interaction with reduced TiO<sub>2</sub> for highly stable photocatalytic CO<sub>2</sub> reduction into CO. *J. CO<sub>2</sub> Util.* **2023**, *67*, 102324. [[CrossRef](#)]
36. Han, B.; Hu, Y. Engineering. MoS<sub>2</sub> as a co-catalyst for photocatalytic hydrogen production from water. *Energy Sci. Eng.* **2016**, *4*, 285–304. [[CrossRef](#)]
37. Tien, T.-M.; Chen, E.L. S-Scheme System of MoS<sub>2</sub>/Co<sub>3</sub>O<sub>4</sub> Nanocomposites for Enhanced Photocatalytic Hydrogen Evolution and Methyl Violet Dye Removal under Visible Light Irradiation. *Coating* **2023**, *13*, 80. [[CrossRef](#)]
38. Sun, M.; Wang, Y.; Fang, Y.; Sun, S.; Yu, Z. Compounds. Construction of MoS<sub>2</sub>/CdS/TiO<sub>2</sub> ternary composites with enhanced photocatalytic activity and stability. *J. Alloys Compd.* **2016**, *684*, 335–341. [[CrossRef](#)]
39. Wang, Y.; Chen, W.; Chen, X.; Feng, H.; Shen, D.; Huang, B.; Jia, Y.; Zhou, Y.; Liang, Y. Effect of sulfur source on photocatalytic degradation performance of CdS/MoS<sub>2</sub> prepared with one-step hydrothermal synthesis. *J. Environ. Sci.* **2018**, *65*, 347–355. [[CrossRef](#)] [[PubMed](#)]
40. Wang, Y.; Sun, M.; Fang, Y.; Sun, S.; He, J. Ag<sub>2</sub>S and MoS<sub>2</sub> as dual, co-catalysts for enhanced photocatalytic degradation of organic pollutions over CdS. *J. Mater. Sci.* **2016**, *51*, 779–787. [[CrossRef](#)]
41. Ghasemipour, P.; Fattahi, M.; Rasekh, B.; Yazdian, F. Developing the ternary ZnO doped MoS<sub>2</sub> nanostructures grafted on CNT and reduced graphene oxide (RGO) for photocatalytic degradation of aniline. *Sci. Rep.* **2020**, *10*, 4414. [[CrossRef](#)] [[PubMed](#)]
42. Ritika, M.K.; Umar, A.; Mehta, S.K.; Singh, S.; Kansal, S.K.; Fouad, H.; Alothman, O.Y. Rapid solar-light driven superior photocatalytic degradation of methylene blue using MoS<sub>2</sub>-ZnO heterostructure nanorods photocatalyst. *Materials* **2018**, *11*, 2254. [[CrossRef](#)]
43. El Malti, W.; Hijazi, A.; Abou Khalil, Z.; Yaghi, Z.; Medlej, M.K.; Reda, M. Comparative study of the elimination of copper, cadmium, and methylene blue from water by adsorption on the citrus Sinensis peel and its activated carbon. *RSC Adv.* **2022**, *12*, 10186–10197. [[CrossRef](#)]
44. Mirsalari, S.A.; Nezamzadeh-Ejhieh, A.; Massah, A.R.; Research, P. A designed experiment for CdS-AgBr photocatalyst toward methylene blue. *Env. Sci. Pollut. Res. Int.* **2022**, *29*, 33013–33032. [[CrossRef](#)] [[PubMed](#)]

45. Chen, L.; He, C.; Yin, J.; Chen, S.; Zhao, W.; Zhao, C. Clearance of methylene blue by CdS enhanced composite hydrogel materials. *Environ. Technol.* **2022**, *43*, 355–366. [[CrossRef](#)] [[PubMed](#)]
46. Jing, C.; Zhang, Y.; Zheng, J.; Ge, S.; Lin, J.; Pan, D.; Naik, N.; Guo, Z. In-situ constructing visible light CdS/Cd-MOF photocatalyst with enhanced photodegradation of methylene blue. *Particuology* **2022**, *69*, 111–122. [[CrossRef](#)]

**Disclaimer/Publisher’s Note:** The statements, opinions and data contained in all publications are solely those of the individual author(s) and contributor(s) and not of MDPI and/or the editor(s). MDPI and/or the editor(s) disclaim responsibility for any injury to people or property resulting from any ideas, methods, instructions or products referred to in the content.